Supporting Information for "Disentangling The Causes of Discrepancies In Simulated Immersion-mode Ice Nucleating Particles"

Aishwarya Raman [1], Elise K. Wilbourn [2,3], Naruki Hiranuma [2], Mikhail S. Pekour[1], Susannah M. Burrows[1]

[1]Pacific Northwest National Lab, Richland, WA

[2]Dept. of Life, Earth and Environmental Sciences, West Texas A&M University,Canyon, TX

[3]*Now at Sandia National Laboratories,Livermore, CA

Contents of this file

1. Text S1 to S11
2. Figures S1 to S3
3. Dataset S1
4. Tables S1 to S4

Text S1. Sampling location

INP and aerosol measurements were sampled at the Department of Energy (DOE) Atmospheric Radiation Measurement (ARM) observatory in Graciosa Island, Azores (39.09°N, 28.02°W) (Hiranuma et al., 2022; Uin et al., 2020). The observatory is located in a remote marine setting in the Eastern North Atlantic (ENA), ca. 1500 km away from the nearest continental land mass and the island is surrounded by ocean waters rich in seasonal phytoplankton (Zawadowicz et al., 2021). The marine boundary layer at ENA is impacted by the oceanic emissions of sea spray aerosol and long-range-transported dust and continental aerosol (Logan et al., 2014).

Text S2. List of aerosol and INP measurements

Table S1 provides a summary of aerosol and INP instruments along with the particle size range detected by the instrument.

Text S3. Deriving total aerosol surface area From nephelometer

The integrating nephelometer is an instrument in the ARM Aerosol Observing System (AOS) at the ENA observatory that measures aerosol optical scattering in three wavelengths

Table S1. Measurable particle size range for individual instruments used in this study.

Instrument	Manufacturer-Model	Measurable size range (nm)
Nephelometer	TSI-3563	10-10000 (Volume Equivalent Diameter)
SEM-EDX	JEOL-JSM-6010LA	250-8000 (Area-equivalent Diameter – Aerodynamic Diameter)
PINE	Bilfinger Noell - PINE-3	30-3000 (Aerodynamic Diameter)

(700 nm, 500 nm, and 450 nm) at ambient relative humidity conditions. In this study, we use the total aerosol surface area per unit volume (S_{aer} in units of $m^2\,m^{-3}$) derived using the aerosol scattering coefficients at the wavelength λ= 450 nm.

$$S_{aer} = 4\frac{b_{sp}}{Q}\,, \tag{1}$$

where b_{sp} is the aerosol scattering coefficient (m^{-1}) measured by the nephelometer, and Q is the total aerosol scattering efficiency assumed based on the characteristic total aerosol distribution and composition. The AOS nephelometer alternates between a 1 µm impactor and a 10 µm impactor for measuring scattering from submicron and super-micron aerosol size distributions. Because ice nucleating efficiency of aerosol particles is directly proportional to their total surface area, we use scattering measurements only for larger particles from the 10 µm impactor with an aerodynamic diameter size cut off at 10 µm.

Approximations for Q values are based on the aerosol size distribution dominating scattering at a given location and time. Following DeMott et al. (2016), we assumed $Q = 3.0$ for marine aerosols with dominant scattering from submicron particles. Testa et al. (2021) estimated a range of Q values from 0.58–2.31 for sub- and supermicron particle size distributions at $\lambda = 450$ nm. To account for uncertainties in S_{aer} due to uncertainties in Q, we calculated S_{aer} for $Q = 0.58$, $Q = 2.0$, and $Q = 3.0$ using Equation 1.

Text S4. Particle-Type Classification using Scanning Electron Microscopy with Energy-Dispersive X-ray Analysis

Particle composition of aerosol particles collected from the Eastern North Atlantic (ENA) site was measured using the scanning electron microscopy energy dispersive X-ray spectroscopy (SEM-EDX) system (Jeol, last accessed, August 11 2022). SEM-EDX technology

is further described in the described in the manufacturer's online document (JEOL, 2022). Briefly, aerosol particles captured on polycarbonate filters were assessed with the SEM-EDX instrument to determine the atomic percentage (atomic %) of 13 elements (N, O, Na, Mg, Al, Si, P, S, Cl, K, Ca, Mn, and Fe). All analyses were consistently carried out with the electron beam accelerating voltage of 20 keV and a 10 mm distance from the underside of the SEM objective lens to the specimen surface. Since the particles were collected on polycarbonate filters, it was not possible to determine organic chemical composition. Instead, SEM-EDX data were used to determine the presence or absence of dust and/or sea salt particles. In addition, the relative age of the particle population was assessed by the ratio of Na+ to Cl-. For instance, this ratio in freshly emitted sea salt is typically much closer to that in the "aged" sea spray aerosols, which show depletion of chloride ions via reactions with sulfuric and nitric acid to form HCl aerosols (Zhang et al., 2010). Although this SEM-EDX method is qualitative rather than a quantitative measurement, atomic % and Na:Cl ratios can be used to determine the approximate amount of local, freshly emitted sea spray aerosols present at the ENA site as compared with the percentage of particles that are aged mixtures with dust.

A total of 400 aerosol particles (i.e., 4 filter samples and 100 particles per sample) in the observed diameter range up to 4.6 µm was analyzed on a single-particle basis (particle size distribution data is available upon request). It should be noted that, while the lower limit of particle collection is nominally 0.2 µm based on filter pore size, the lower detection limit for the SEM method employed here is 0.5 µm particle diameter. Single particles were selected on each filter to analyze particle composition, with at least 100 particles to represent the population chemical composition and allow for classification of major particle groups. All particles were randomly selected with a strategy of selecting 25 particles over the 128 µm x 96 µm cross-sections (x4). No specific particle size or shape was selected for analysis. Instead, a range of sizes and shapes was targeted to give the best approximation of overall population chemistry. SEM-EDX is a time-intensive and labor-intensive process, so its application during this study was limited. For this reason, a few time periods were chosen to study in greater detail. These periods contrast with one another in terms of ice-nucleating particle (INP) concentration and heat sensitivity (not shown). Each filter was collected for approximately four days and high INP periods were chosen based on complementary offline immersion freezing measurements. The same filters were analyzed with the offline cold stage-supported freezing assay measurements and SEM-EDX.

Data for each filter sample is available in Dataset S1. This table also shows the composition of samples determined with SEM-EDX. The atomic % of 13 different elements was used to classify particles as either salt-dominant (and thus marine-dominant) or dust-dominant (and thus terrestrial-dominant), classified based on methods presented in Figure 5 of Hiranuma et al. (2013).

The four sample periods were chosen to represent both high-INP periods ($0.39\,\mathrm{L}^{-1}$ and $0.33\,\mathrm{L}^{-1}$ at $-25\,^{\circ}\mathrm{C}$ for ENA2020-11 and ENA2020-14, respectively) and low INP periods ($0.04\,\mathrm{L}^{-1}$ and INP $0.1\,\mathrm{L}^{-1}$ at $-25\,^{\circ}\mathrm{C}$ for ENA2020-28 and ENA2020-36, respectively). Additionally, samples ENA2020-14 and ENA2020-36 showed heat sensitivity at temperatures above $-15\,^{\circ}\mathrm{C}$, while samples ENA2020-11 and ENA2020-28 did not heat sensitivity.

Most of the samples were dominated by salt-dominant particles, while ENA2020-11 had a greater percentage of dust-dominant particles. It is well-known that aluminosilicate mineral dust is capable of acting as an INP (Zimmermann et al., 2008) and generally does not show sensitivity to the heating method employed herein (Zolles et al., 2015). Although it is difficult to draw conclusions from a single sample, the high INP concentrations seen during this time period (and confirmed with online methods) could be due to higher concentrations of mineral dust in this sample than the others analyzed.

As seen in Dataset S1, the Na:Cl ratio in samples from ENA is consistently around 2. This number suggests that the samples are traveling from some distance and aging before reaching the site. However, since the site is 1500 km from the nearest sources of terrestrial material, sea spray aerosols must make up some proportion of the aerosols present at the site. The mixture of sea spray aerosols, dust, and organic material leads to a unique relationship between cloud condensation nuclei (CCN) and INPs at ENA that is heretofore unobserved at any other marine or terrestrial sites and suggests a common source for both types of aerosols. This relationship warranty further study and will be discussed in future papers.

Text S5. Comparison of SEM-EDX analysis to a previous aerosol classification study at ENA

Figure S1 shows the comparison of previous SEM-EDX-based particle composition data to our data for particle samples collected at the same location in ENA. Briefly, Knopf et al. (2022) (K22 hereafter) conducted the SEM-EDX-derived cluster analysis for the identifi-

cation of particle-type classes present in particle samples collected during the Aerosol and cloud experiments in ENA (ACE-ENA) campaign in June and July 2017. Panels (a–d) display the normalized atomic % of 13 selected elements for the four particle-type classes from ACE-ENA (adapted from K22). The representative particle types include (a) processed sea salt with mineral dust, sulfur, and organic matter, (b) sea salt particles, (c) processed sea salt with mineral dust, and (d) organic matter–chlorine-containing particles. Contrarily, Panels (e-h) show non-clustered atomic % of the same elements for individual samples from the Examining INP from ENA (ExINP-ENA) campaign in 2020 (i.e., Dataset S1). With notably high normalized atomic % of oxygen atoms (¿ 55 %), all ExINP-ENA samples indicate the inclusion of highly oxygenated sea salt- and dust-including particles. This oxygen-enriched feature can also be seen in Fig. S1a (processed sea salt with 50% oxygen atomic %). Likewise, the inclusion of sea salt- and dust-makers (i.e., Na, Mg, Cl, Al, and Ca) are commonly found in both ACE-ENA and ExINP-ENA samples. Although all aerosol particle populations analyzed from ExINP-ENA contained sea salt, all particles also contained dust in variable concentrations, and there was no relationship between air mass origin (determined by back-trajectory analysis but not shown) and dust content, indicating that all aerosol populations at ENA during the sampling period contained mixed sea spray aerosols and continental aerosols. While organic content could not be measured by SEM-EDX due to the background signal from the polycarbonate filter substrate, it is highly likely that the sea spray aerosols (indicated by the presence of Na and Cl in SEM-EDX) contained organic material in addition to salts since sea spray aerosols contain both salts and organic material. Such a high degree of mixed components can in part explain the observed indication of chloride depletion (Na:Cl ratios ¿ 1.9 in Table S1) and particle aging. On the other hand, our results generally suggest less inclusion of K, Mn, and Fe and more pronounced P inclusion in ExINP-ENA particle samples (especially ENA2020-18 and ENA2020-36) than ACE-ENA samples. While the source of observed discrepancies between the two studies is uncertain, we presume the use of different inlet and filter impactor systems (and resulting different sizes of collected particles) can act as the source besides different air mass sources. In fact, the K22 particle samples were collected using a micro orifice uniform deposit impactor with a 50% cut-size of 0.56 µm in aerodynamic diameter (Dae) whereas the particle sampling system employed for ExINP-ENA allowed the collection of particles up to 8 µm in Dae.

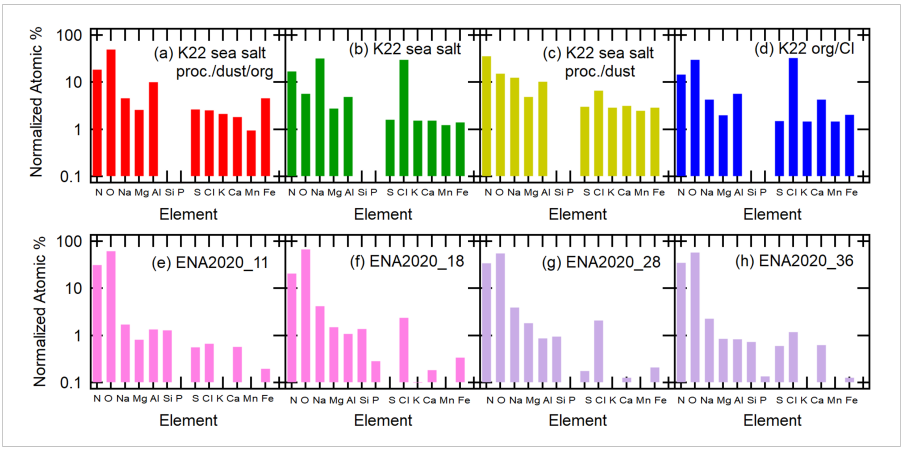

Figure S1. Figure S1. SEM-EDX-based particle elemental composition data from ACE-ENA 2017 (a-d) and ExINP-ENA 2020 (e-h)

Although it is apparent that the population of aerosols at ENA is unique from other marine sites, the physicochemical properties are not well understood and warrant much closer study. Characterization of the mixing state of particles should be examined to compare with other, better understood sites. Glassy aerosols may act as INPs, so the viscosity should also be studied (Berkemeier et al., 2014). Finally, as many of the best INPs are organics with biological origin, samples from ENA could be explored using both chemical characterization methods including mass spectrometry and biological characterization methods including proteomic and metabolomic methods to discover whether the biological aerosols (Huang et al., 2021) present at the site are undergoing processes distinct to this site. The differences between our study and (Knopf et al., 2022) can be attributed to many factors including, but not limited to, underestimation of sea spray INP concentrations in M18 (e.g., (Cornwell et al., 2021)), different air masses, and different inlet and filter impactor systems.

Text S6. Using Poisson statistics to determine temperature-dependent errors from online methods

The temperature uncertainty for PINE-measured INPs was estimated to be ±1.5°C (Hiranuma et al., 2022). This temperature uncertainty is mainly due to the inhomogeneity in the temperature readings at different locations inside the PINE chamber during the expansion run (Möhler et al., 2021). We measured the INP number concentrations of ambient and filtered air with the PINE instrument. Because INP concentrations vary with temperature, the errors associated with INPs are also temperature dependent. We estimate the temperature-

dependent errors in INP concentrations at four temperatures (−16 °C,−21 °C,−26 °C, and −31 °C). For closure analysis in the main text, we use errors obtained for −31 °C measurements to represent temperature-dependent errors in −29 °C INP measurements.

These errors were calculated from measurements of large particles detected during normal sampling procedures and those detected during times when the chamber was filled with filtered air (Krishnamoorthy & Lee, 2013). The filtered air represented the background INP concentrations, and the mean and error were calculated with Poisson statistics based on equations 6 and 8 from Krishnamoorthy and Lee (2013). The statistical validity of the calculated mean was ensured by comparison with the calculated Z statistic, which showed the statistical significance of data points above −16 °C. To ensure the calculated error is applicable to the entire dataset, background and ambient measurements were made on at least three separate days. The 95% CIs at −21 °C, −25 °C, and −31 °C were 1.56 ± 0.93, 6.05 ± 1.41, and 23.28 ± 3.81 L^{-1}, respectively.

Data Set S1. SEM-EDX

Filter name	Start date/time	End date/time	Sea salt percent	Dust percent	Na/CL ratio
ENA2020-11	10/11/20 14:24	10/14/20 15:30	29 ±21	68 ±14	2.73 ±0.20
ENA2020-18	10/17/20 15:24	10/20/20 14:24	70 ±16	30 ±16	1.94 ±0.08
ENA2020-28	11/1/20 13:47	11/4/20 16:03	85 ±13	15 ±18	1.91 ±0.06
ENA2020-36	11/15/20 16:42	11/18/20 13:24	56 ±16	42 ±16	2.00 ±0.09

Table S2. Four samples collected on polycarbonate filters were analyzed with SEM-EDX to determine the percentage of particles primarily composed of salt (Na and Mg) and the percentage of particles primarily composed of dust (Al, Si, and Ca). The Na to Cl ratio is also presented. All data points are average ± standard error, n = 100.

Text S7. EAMv1 model description

We use the U.S. DOE Energy Exascale Earth System Atmosphere Model version 1 (EAMv1) (Neale et al., 2010; Golaz et al., 2022) with the modal aerosol module with four log-normal modes (MAM4) (Wang et al., 2020) to simulate the size-resolved aerosol composition inputs for the INP parameterizations. Here, we use interstitial and cloud-borne aerosol simulated using the MAM4 prognoses. Sea spray aerosol emissions in MAM4 are based on Mårtensson et al. (2003) parameterization for particle diameters from 0.020 µm to 2.5 µm and Monahan et al. (1986) from 2.5 µm to 10 µm. Marine Organic Aerosol (MOAs) in sea spray are simulated by the Organic Compounds from Ecosystems to Aerosols: Natural Films and Interfaces via Langmuir Molecular Surfactants (OCEANFILMS) emission source function (Burrows et al., 2018, 2022). Dust emissions are simulated as a function of threshold surface wind friction velocity and soil type (Mahowald et al., 2006) and the size distribution of dust follows Zender et al. (2003). Detailed evaluations of MAM4 aerosol in EAMv1 are available in Wang et al. (2020).

Text S8. Immersion-mode INP parameterizations

To estimate sea spray INP concentrations, we use the McCluskey et al. (2018) $n_s(T)$ parameterization along with the total sea spray surface area (M18). For mineral dust, we select multiple $n_s(T)$ parameterization fits discussed in Boose et al. (2016) because of the substantial uncertainties in mineral dust ice nucleating abilities in the literature (e.g. Boose et

al., 2016; Atkinson et al., 2013; Kanji et al., 2017). Specifically, we select the $n_s(T)$ fits for Moroccan and Peloponnese dust samples that possess the highest and lowest ice nucleating abilities, respectively, as shown in Figure 5 of Boose et al. (2016). These sites are also closer to ENA (a few thousand kilometers). For representing the median $n_s(T)$ estimates, we select the Ullrich et al. (2017) parameterization (UL17) which was developed using the global dust samples in Aerosol Interaction and Dynamics in the Atmosphere (AIDA) chamber ice nucleation experiments. To account for the particle size dependence of INPs, we also use size-dependent $n_s(T)$ parameterizations for dust adopted from Reicher et al. (2019) (REI19 sub-micron and REI19 super-micron). We compare different $n_s(T)$ in Text S9.

Text S9. Ice Nucleation Active Site Densities at ENA

Ice-nucleation-active site density (INAS, $n_s(T)$) has been commonly used to quantify the ice nucleation efficiency of single minerals (e.g. McCluskey et al., 2019; Ullrich et al., 2017; Boose et al., 2016; Mitts et al., 2021). $n_s(T)$ represents the INP concentrations that are normalized by the dry aerosol surface area. Figure S2 compares several temperature dependent $n_s(T)$ parameterizations for dust and sea spray INPs. M18 $n_s(T)$ estimates for sea spray INPs (blue line, Figure S2) are lower by at least three orders of magnitude than most dust $n_s(T)$ curves, consistent with the previous findings that dust is more ice active than sea spray aerosols (DeMott et al., 2016).

On the other hand, dust $n_s(T)$ calculated using different parameterizations differ by several orders of magnitude, even though all represent the same INP category of dust. For example, at $-20°$C, dust $n_s(T)$ parameterizations range from $1.0 \times 10^8\,\mathrm{m}^{-2}$ to $1.0 \times 10^{11}\,\mathrm{m}^{-2}$. The $n_s(T)$ estimates for airborne dust samples (B16 Peloppenesse, REI) are generally lower than those for surface dust sediments (UL17) and milled samples (B16 Morocco), which implies that the atmospheric transformation during long-range transport affects the INP efficiency of dust, consistent with previous studies (Boose et al., 2016).

Text S10. Aerosol-INP closure Figure S2 illustrates a schematic outline of the INP error decomposition method we use in this study.

We use the metric Modified normalized bias (MNB) to calculate the closure error. MNB is symmetric, ranges between -2 (under prediction) and 2 (over prediction), and the normalization makes it less sensitive to outliers compared to other error metrics such as the root mean squared error. MNB values close to zero indicate the best agreement between the two

INP type	$n_s(T)$	**Aerosol property**	**Sample type and conditions**
Sea spray	M18 (McCluskey et al., 2018)	Sea spray aerosol surface area concentration (0.08 µm to 10 µm) [$m^{-2}\,m^{-3}$]	Background sea spray samples collected at Mace Head station in clean marine conditions.
Dust	B16 Peloponnese (Boose et al., 2016)	Dust aerosol surface area concentration (0.08 µm to 10 µm) [$m^{-2}\,m^{-3}$]	Airborne sample from a single dust event collected in Peloponnese; dominated by calcite.
Dust	B16 Morocco (Boose et al., 2016)	Dust aerosol surface area concentration (0.08 µm to 10 µm) [$m^{-2}\,m^{-3}$]	Surface sample collected in Morocco and milled for IN experiments; dominated by Quartz.
Dust	UL17 (Ullrich et al., 2017)	Dust aerosol surface area concentration (0.08 µm to 10 µm) [$m^{-2}\,m^{-3}$]	Ground samples of desert dust from different locations.
Dust	REI19 supermicron (Reicher et al., 2019)	Dust aerosol surface area concentration (1 µm to 10 µm) [$m^{-2}\,m^{-3}$]	Airborne dust particles collected during different dust events in the eastern Mediterranean.

Table S3. Immersion-mode INP parameterizations used in this study.

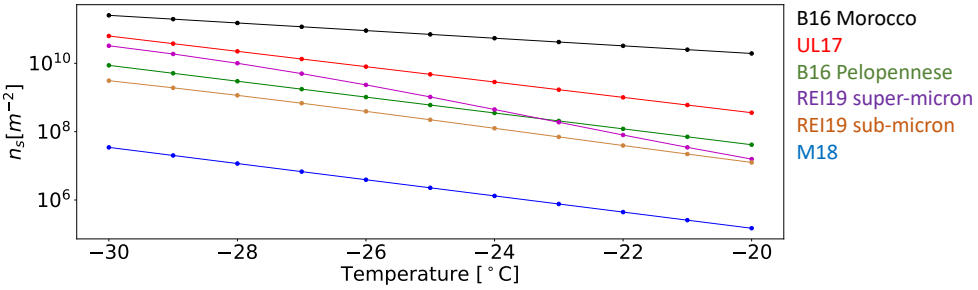

Figure S2. Ice active site density parameterizations for dust and sea spray populations plotted against freezing temperatures.

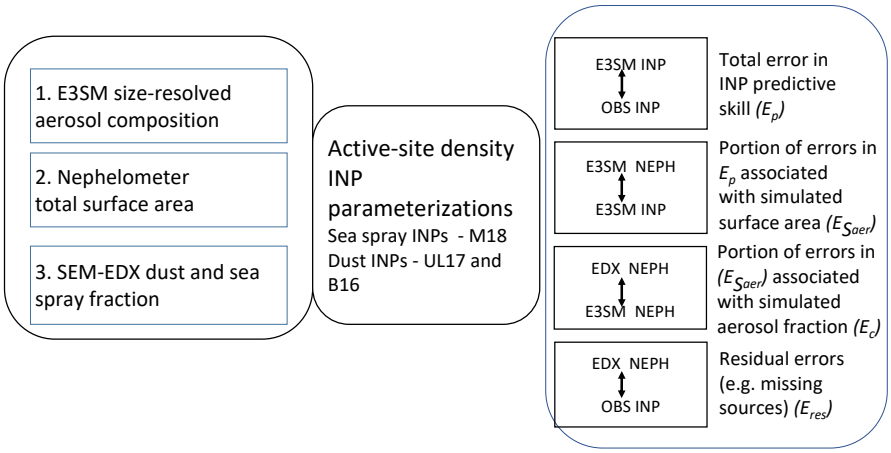

Figure S3. Schematic outline of the INP closure analysis

quantities. Eskes et al. (2015) used a similar metric called modified normalized mean bias (MNMB) to validate the predictability of atmospheric composition in the The Monitoring Atmospheric Composition and Climate (MACC) global analysis and forecast system. The difference between the metric MNB and MNMB is that MNMB is calculated as two times the average of MNB.

Text S11. Uncertainty propagation

We quantify the uncertainty in each error source given the independent aerosol and INP measurements. Here, we describe the uncertainty propagation technique to quantify uncertainties in the total INP discrepancy due to uncertainties in aerosol composition and residual sources. We define the uncertainty in E_c ($\partial \mathrm{E_c}$) due to uncertainties in SEM-EDX aerosol classification as:

Table S4. Closure error for the combined INPs from M18 and different dust INP parameterizations at different temperatures. INP concentrations are calculated using the observed aerosol fraction and total surface area from EDX and the nephelometer, respectively.

Temp	INP parameterization	Closure error temporal mean
$-29°C$	M18 + B16 Morocco	0.98
$-29°C$	M18 + UL17	0.89
$-29°C$	M18 + REI19 super	0.79
$-29°C$	M18 + B16 Pelopennese	0.45
$-27°C$	M18 + B16 Morocco	0.98
$-27°C$	M18 + UL17	0.89
$-27°C$	M18 + REI19 super	0.70
$-27°C$	M18 + B16 Pelopennese	0.39
$-25°C$	M18 + B16 Morocco	0.97
$-25°C$	M18 + UL17	0.70
$-25°C$	M18 + REI19 super	0.11
$-25°C$	M18 + B16 Pelopennese	-0.15
$-22°C$	M18 + B16 Morocco	0.94
$-22°C$	M18 + UL17	0.32
$-22°C$	M18 + REI19 super	-0.27
$-22°C$	M18 + B16 Pelopennese	-0.15

$$\delta \mathrm{E_c(T)} = \frac{\partial \mathrm{E_c(T)}}{\partial \mathrm{INP_{EDX\ NEPH}(T)}} \left(\frac{\partial \mathrm{INP_{EDX\ NEPH}(T)}}{\partial \mathrm{e_{du}}}\, \partial \mathrm{e_{du}} + \frac{\partial \mathrm{INP_{EDX\ NEPH}(T)}}{\partial \mathrm{e_{ss}}}\, \partial \mathrm{e_{ss}} \right)$$
$$= \frac{-2\ \overline{\mathrm{INP_{E3SM\ NEPH(T)}}}}{\left(\overline{\mathrm{INP_{E3SM\ NEPH(T)}}} + \overline{\mathrm{INP_{EDX\ NEPH(T)}}}\right)^2} \Big(\overline{n_{s(\mathrm{du})}(T) S_{\mathrm{aer(Neph)}} \delta e_{\mathrm{du}}}$$
$$+ \overline{n_{s(ss)}(T) S_{\mathrm{aer(Neph)}} \delta e_{\mathrm{ss}}} \Big), \quad (2)$$

where $\frac{\partial \mathrm{INP_{EDX\ NEPH}(T)}}{\partial \mathrm{e_{du}}}$ is the change in predicted INP concentrations using observed aerosol properties due to the uncertainties in dust fraction measured by SEM-EDX, $\partial \mathrm{INP_{EDX\ NEPH}(T)} \overline{\partial \mathrm{e_{ss}}}$ is the change in predicted INP concentrations using observed aerosol properties due to the uncertainties in sea spray fraction measured by SEM-EDX, $n_{s(\mathrm{du})}(T)$ and $n_{s(\mathrm{ss})}(T)$ denote the temperature-dependent ice-active site density parameterizations for dust and sea spray, respectively, $S_{\mathrm{aer(Neph)}}$ denotes the nephelometer-based total surface area, and e_{du} and e_{ss} denote the errors in EDX-derived dust and sea spray fractions, which can arise from various factors such as electron intensity stability, beam spot size accuracy, detected X-ray counting efficiency, and magnification or focus precision. We describe the notation and the INP calculations in Table **??**.

We define the uncertainty in E_{res} ($\partial \mathrm{E_{res}}$) due to temperature-dependent errors in PINE INP measurements (δ INP OBS) as:

$$\delta \mathrm{E_{res}} = \frac{\partial \mathrm{E_{res}}}{\partial \mathrm{INP_{INP\ OBS}}}\ \delta \mathrm{INP_{INP\ OBS}}$$
$$= \frac{-2\ \overline{\mathrm{INP_{EDX\ NEPH}}}(\mathrm{T})}{\left(\overline{\mathrm{INP_{EDX\ NEPH}}}(\mathrm{T}) + \overline{\mathrm{INP_{OBS}}}(\mathrm{T})\right)^2}\ \delta \mathrm{INP_{INP\ OBS}}, \quad (3)$$

Due to the sparse availability of SEM-EDX observations for the campaign time period, we use the mean INP concentrations of all SEM-EDX samples to estimate MNB for error sources E_c and E_{res}. For the other error components $E_{S_{aer}}$ and E_p, we estimate MNB using the 6-hourly averaged INP concentrations.

References

Atkinson, J. D., Murray, B. J., Woodhouse, M. T., Whale, T. F., Baustian, K. J., Carslaw, K. S., ... Malkin, T. L. (2013). The importance of feldspar for ice nucleation by mineral dust in mixed-phase clouds. *Nature*, *498*(7454), 355–358.

Berkemeier, T., Shiraiwa, M., Pöschl, U., & Koop, T. (2014). Competition between water uptake and ice nucleation by glassy organic aerosol particles. *Atmospheric Chemistry and Physics*, *14*(22), 12513–12531.

Boose, Y., Welti, A., Atkinson, J., Ramelli, F., Danielczok, A., Bingemer, H. G., ... Lohmann, U. (2016). Heterogeneous ice nucleation on dust particles sourced from nine deserts worldwide–part 1: Immersion freezing. *Atmospheric Chemistry and Physics*, *16*(23), 15075–15095.

Burrows, S. M., Easter, R., Liu, X., Ma, P.-L., Wang, H., Elliott, S. M., ... Rasch, P. J. (2018). Oceanfilms sea-spray organic aerosol emissions–part 1: implementation and impacts on clouds. *Atmospheric Chemistry and Physics Discussions*, 1–27.

Burrows, S. M., Easter, R. C., Liu, X., Ma, P.-L., Wang, H., Elliott, S. M., ... Rasch, P. J. (2022). Oceanfilms (organic compounds from ecosystems to aerosols: Natural films and interfaces via langmuir molecular surfactants) sea spray organic aerosol emissions–implementation in a global climate model and impacts on clouds. *Atmospheric Chemistry and Physics*, *22*(8), 5223–5251.

Cornwell, G. C., McCluskey, C. S., DeMott, P. J., Prather, K. A., & Burrows, S. M. (2021). Development of heterogeneous ice nucleation rate coefficient parameterizations from ambient measurements. *Geophysical Research Letters*, *48*(23), e2021GL095359.

DeMott, P. J., Hill, T. C., McCluskey, C. S., Prather, K. A., Collins, D. B., Sullivan, R. C., ... others (2016). Sea spray aerosol as a unique source of ice nucleating particles. *Proceedings of the National Academy of Sciences*, *113*(21), 5797–5803.

Eskes, H., Huijnen, V., Arola, A., Benedictow, A., Blechschmidt, A.-M., Botek, E., ... others (2015). Validation of reactive gases and aerosols in the macc global analysis and forecast system. *Geoscientific model development*, *8*(11), 3523–3543.

Golaz, J.-C., Van Roekel, L. P., Zheng, X., Roberts, A. F., Wolfe, J. D., Lin, W., ... others (2022). The doe e3sm model version 2: overview of the physical model and initial model evaluation. *Journal of Advances in Modeling Earth Systems*, *14*(12).

Hiranuma, N., Brooks, S. D., Moffet, R. C., Glen, A., Laskin, A., Gilles, M. K., ... McFarquhar, G. (2013). Chemical characterization of individual particles and residuals of cloud droplets and ice crystals collected on board research aircraft in the isdac 2008 study. *Journal of Geophysical Research: Atmospheres*, *118*(12), 6564–6579.

Hiranuma, N., Wilbourn, E. K., & Lacher, L. (2022). *Examining the ice-nucleating particles from the eastern north atlantic (exinp-ena) field campaign report* (Tech. Rep.). Oak

Ridge National Lab.(ORNL), Oak Ridge, TN (United States). Atmospheric ....

Huang, S., Hu, W., Chen, J., Wu, Z., Zhang, D., & Fu, P. (2021). Overview of biological ice nucleating particles in the atmosphere. *Environment International*, *146*, 106197.

Jeol. (last accessed, August 11 2022). Scanning electron microscope a to z: Basic knowledge for using the sem. In *Jeol*.

Kanji, Z. A., Ladino, L. A., Wex, H., Boose, Y., Burkert-Kohn, M., Cziczo, D. J., & Krämer, M. (2017). Overview of ice nucleating particles. *Meteorological Monographs*, *58*, 1–1.

Knopf, D. A., Charnawskas, J. C., Wang, P., Wong, B., Tomlin, J. M., Jankowski, K. A., ... others (2022). Micro-spectroscopic and freezing characterization of ice-nucleating particles collected in the marine boundary layer in the eastern north atlantic. *Atmospheric chemistry and physics*, *22*(8), 5377–5398.

Krishnamoorthy, K., & Lee, M. (2013). New approximate confidence intervals for the difference between two poisson means and comparison. *Journal of Statistical Computation and Simulation*, *83*(12), 2232–2243.

Logan, T., Xi, B., & Dong, X. (2014). Aerosol properties and their influences on marine boundary layer cloud condensation nuclei at the arm mobile facility over the azores. *Journal of Geophysical Research: Atmospheres*, *119*(8), 4859–4872.

Mahowald, N. M., Muhs, D. R., Levis, S., Rasch, P. J., Yoshioka, M., Zender, C. S., & Luo, C. (2006). Change in atmospheric mineral aerosols in response to climate: Last glacial period, preindustrial, modern, and doubled carbon dioxide climates. *Journal of Geophysical Research: Atmospheres*, *111*(D10).

Mårtensson, E., Nilsson, E., de Leeuw, G., Cohen, L., & Hansson, H.-C. (2003). Laboratory simulations and parameterization of the primary marine aerosol production. *Journal of Geophysical Research: Atmospheres*, *108*(D9).

McCluskey, C. S., DeMott, P. J., Ma, P.-L., & Burrows, S. M. (2019). Numerical representations of marine ice-nucleating particles in remote marine environments evaluated against observations. *Geophysical Research Letters*, *46*(13), 7838–7847.

McCluskey, C. S., Hill, T. C., Sultana, C. M., Laskina, O., Trueblood, J., Santander, M. V., ... others (2018). A mesocosm double feature: Insights into the chemical makeup of marine ice nucleating particles. *Journal of the Atmospheric Sciences*, *75*(7), 2405–2423.

Mitts, B. A., Wang, X., Lucero, D. D., Beall, C. M., Deane, G. B., DeMott, P. J., & Prather, K. A. (2021). Importance of supermicron ice nucleating particles in nascent sea spray.

Geophysical Research Letters, *48*(3), e2020GL089633.

Möhler, O., Adams, M., Lacher, L., Vogel, F., Nadolny, J., Ullrich, R., ... others (2021). The portable ice nucleation experiment (pine): a new online instrument for laboratory studies and automated long-term field observations of ice-nucleating particles. *Atmospheric Measurement Techniques*, *14*(2), 1143–1166.

Monahan, E., Spiel, D., & Davidson, K. (1986). A model of marine aerosol generation via whitecaps and wave disruption. *Oceanic whitecaps: And their role in air-sea exchange processes*, 167–174.

Neale, R. B., Chen, C.-C., Gettelman, A., Lauritzen, P. H., Park, S., Williamson, D. L., ... others (2010). Description of the ncar community atmosphere model (cam 5.0). *NCAR Tech. Note NCAR/TN-486+ STR*, *1*(1), 1–12.

Reicher, N., Budke, C., Eickhoff, L., Raveh-Rubin, S., Kaplan-Ashiri, I., Koop, T., & Rudich, Y. (2019). Size-dependent ice nucleation by airborne particles during dust events in the eastern mediterranean. *Atmospheric Chemistry and Physics*, *19*(17), 11143–11158.

Testa, B., Hill, T. C., Marsden, N. A., Barry, K. R., Hume, C. C., Bian, Q., ... others (2021). Ice nucleating particle connections to regional argentinian land surface emissions and weather during the cloud, aerosol, and complex terrain interactions experiment. *Journal of Geophysical Research: Atmospheres*, *126*(23), e2021JD035186.

Uin, J., Smith, S., & Springston, S. (2020). *Eastern north atlantic (ena) aerosol observing system (aos) instrument handbook* (Tech. Rep.). Oak Ridge National Lab.(ORNL), Oak Ridge, TN (US). Atmospheric Radiation ....

Ullrich, R., Hoose, C., Möhler, O., Niemand, M., Wagner, R., Höhler, K., ... Leisner, T. (2017). A new ice nucleation active site parameterization for desert dust and soot. *Journal of the Atmospheric Sciences*, *74*(3), 699–717.

Wang, H., Easter, R., Zhang, R., Ma, P.-L., Singh, B., Zhang, K., ... others (2020). Aerosols in the e3sm version 1: New developments and their impacts on radiative forcing. *Journal of Advances in Modeling Earth Systems*, *12*(1), e2019MS001851.

Zawadowicz, M. A., Suski, K., Liu, J., Pekour, M., Fast, J., Mei, F., ... others (2021). Aircraft measurements of aerosol and trace gas chemistry in the eastern north atlantic. *Atmospheric Chemistry and Physics*, *21*(10), 7983–8002.

Zender, C. S., Bian, H., & Newman, D. (2003). Mineral dust entrainment and deposition (dead) model: Description and 1990s dust climatology. *Journal of Geophysical*

Research: Atmospheres, *108*(D14).

Zhang, D., Wang, Z., & Liu, D. (2010). A global view of midlevel liquid-layer topped stratiform cloud distribution and phase partition from calipso and cloudsat measurements. *Journal of Geophysical Research: Atmospheres*, *115*(D4).

Zimmermann, F., Weinbruch, S., Schütz, L., Hofmann, H., Ebert, M., Kandler, K., & Worringen, A. (2008). Ice nucleation properties of the most abundant mineral dust phases. *Journal of Geophysical Research: Atmospheres*, *113*(D23).

Zolles, T., Burkart, J., Hausler, T., Pummer, B., Hitzenberger, R., & Grothe, H. (2015). Identification of ice nucleation active sites on feldspar dust particles. *The Journal of Physical Chemistry A*, *119*(11), 2692–2700.